# First $^{18}$F-Labeled Pentixafor-Based Imaging Agent for PET Imaging of CXCR4 Expression In Vivo

**Andreas Poschenrieder[1], Theresa Osl[1], Margret Schottelius[1], Frauke Hoffmann[1], Martina Wirtz[1], Markus Schwaiger[2], and Hans-Jürgen Wester[1]**

[1]Pharmaceutical Radiochemistry, Technische Universität München, Germany and [2]Nuklearmedizinische Klinik und Poliklinik, Technische Universität München, Ismaningerstr, München, Germany

**Corresponding Author**:
Andreas Poschenrieder
Pharmaceutical Radiochemistry, Technische Universität München,
Walther-Meißner-Str.3, 85748, Garching, Germany;
E-mail: a.poschenrieder@tum.de

**Key Words:** CXCR4, PET, NOTA, $^{18}$F, cancer

**Abbreviations:** Positron emission tomography (PET), dimethyl sulfoxide (DMSO), severe combined immunodeficient (SCID), ethanol (EtOH), phosphate-buffered saline (PBS), electrospray ionization mass spectrometry (ESI-MS)

ABSTRACT

In vivo quantification of CXCR4 expression using [$^{68}$Ga]pentixafor for positron emission tomography (PET) imaging has gained significant clinical interest as CXCR4 plays a fundamental role in oncology and possesses potential prognostic value when overexpressed. To combine the excellent CXCR4-targeting properties of pentixafor-based tracers with the favorable radionuclide properties of $^{18}$F for high-resolution PET imaging, we developed an Al$^{18}$F-labeled 1,4,7-triazacyclononane-triacetic acid (NOTA) analog of pentixather. Al$^{18}$F-labeling of NOTA-pentixather was performed in aqueous dimethyl sulfoxide (DMSO) at pH = 4 (105°C, 15 minutes). CXCR4 affinities were determined in competitive binding assays, and both biodistribution and small-animal PET studies were performed in Daudi lymphoma-bearing mice. Under non-optimized conditions, [$^{18}$F]AlF-NOTA-pentixather was obtained in radiochemical yields of 45.5% ± 13.3% and specific activities of up to 24.8 GBq/$\mu$mol. Compared with [$^{nat}$Ga]pentixafor, [$^{nat}$F]AlF-NOTA-pentixather showed 1.4-fold higher CXCR4 affinity. [$^{18}$F]AlF-NOTA-pentixather displayed high and CXCR4-specific in vivo uptake in Daudi xenografts (13.9% ± 0.8% injected dose per gram [ID/g] at 1 hour post injection [p.i.]). Because of its enhanced lipophilicity (logP = −1.4), [$^{18}$F]AlF-NOTA-pentixather showed increased accumulation in the gall bladder and intestines. However, tumor/background ratios of 7.0 ± 1.2, 2.0 ± 0.3, 2.2 ± 0.4, 16.5 ± 6.5, and 29.2 ± 4 for blood, liver, small intestine, gut, and muscle, respectively, allowed for high-contrast visualization of Daudi tumors using PET (1 hour p.i.). The relatively straightforward radiosynthesis and efficient CXCR4 targeting of [$^{18}$F]AlF-NOTA-pentixather demonstrate the successful implementation of $^{18}$F-complexation chemistry and pentixather-based CXCR4 targeting. Upon pharmacokinetic optimization, this class of tracers holds great promise for future application in humans.

## INTRODUCTION

Overexpression of the chemokine receptor CXCR4 has been linked to cancer development and progression, metastasis and poor prognosis, as well as other pathological conditions, for example, HIV, cardiovascular diseases, and rheumatoid arthritis (1-3). Initially, the development of novel synthetic CXCR4 antagonists was primarily triggered by the discovery of CXCR4 as a coreceptor for HIV-1 entry, leading to the development of potent synthetic CXCL12-analogs such as the tetradecapeptide T140 and the cyclic pentapeptide FC131, as well as the nonpeptidic bicyclam analog AMD3100 (plerixafor), for anti-HIV therapy (4-6).

Based on these lead structures, a variety of CXCR4-targeted agents for molecular imaging applications have been developed in recent years, allowing the sensitive in vivo detection and quantification of CXCR4 expression, and thus, providing increasing insight into the role of CXCR4 in physiology and pathology.

Among the continually increasing numbers of novel CXCR4 imaging agents, including radiolabeled and/or fluorescently labeled T140 (7-12) and AMD3100 analogs (13-17), [$^{68}$Ga]pentixafor (18, 19) holds a prominent position. In contrast to all other CXCR4-targeted imaging probes developed so far, [$^{68}$Ga]pentixafor (formerly termed [$^{68}$Ga]CPCR4.2 compound 1b; Figure 1) shows not only highly efficient CXCR4 targeting in vitro and in vivo but also a suitable pharmacokinetic profile for high-contrast visualization of CXCR4 expression in vivo, that is, rapid renal excretion and low background accumulation. These


ISSN 2379-1381 http://dx.doi.org/10.18383/j.tom.2016.00130

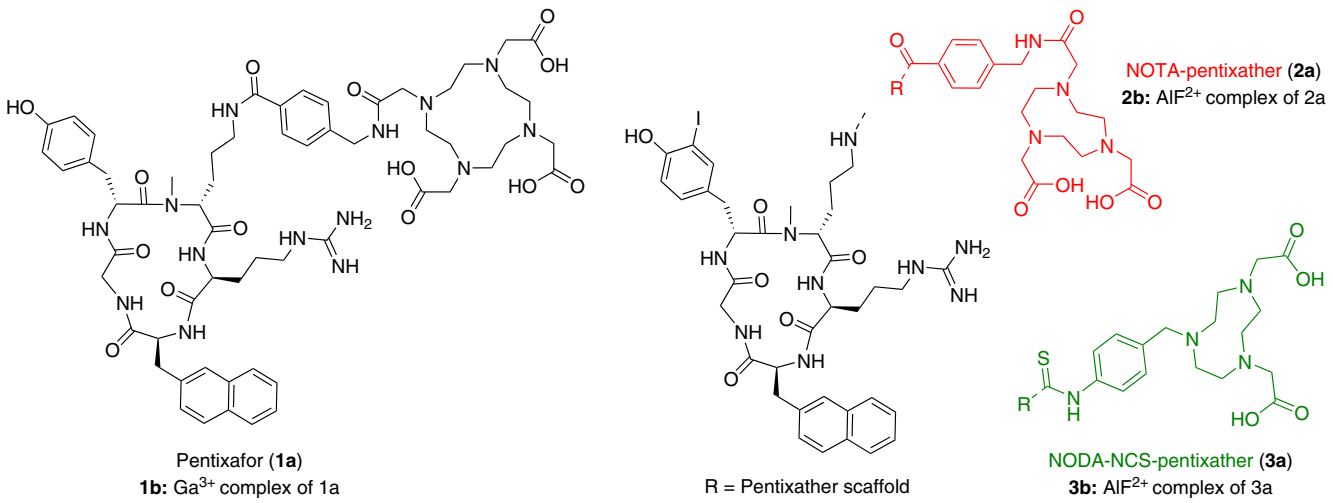


**Figure 1.** Structures of pentixafor (left) and NOTA/NODA-NCS-pentixather (right).

characteristics paved the way for rapid clinical translation of [$^{68}$Ga]pentixafor. Dosimetry and first human studies in patients with lymphoproliferative diseases, such as lymphoma and multiple myeloma, showed highly promising results (20-22), further promoting the entry of [$^{68}$Ga]pentixafor into currently ongoing clinical trials in patients with solid cancer (23), glioblastoma (24), small cell lung cancer (25), and myocardial infarction (26, 27).

However, because the radionuclide properties of $^{18}$F are superior to those of $^{68}$Ga, particularly concerning the positron energy and thus the achievable spatial resolution in positron emission tomography (PET), the motivation toward the development of $^{18}$F-labeled CXCR4 ligands is obvious. To date, only few attempts to develop $^{18}$F-labeled CXCR4 ligands have been reported, and the first tracer, an $^{18}$F-labeled T140 analog, has been reported only recently in 2010 (8). Other attempts include $^{18}$F-labeled radiotracers based on Ac-TC14012 (28) and recently [$^{18}$F]AlF-NOTA chelation of T140 (29). Here, high blood activity levels, occasioned by binding to blood cells, and their very high liver uptake limit the use of $^{18}$F-fluoroacylated T140 derivatives to preclinical applications. In contrast, all currently known $^{18}$F-labeled cyclic pentapeptide analogs show poor CXCR4 affinity, and thus, very low levels of CXCR4-specific accumulation in vivo (30-32).

Therefore, the aim of this study includes the synthesis and evaluation of a novel pentixafor-based $^{18}$F-labeled CXCR4-targeted PET agent, combining an easy $^{18}$F-fluorination chemistry with the excellent CXCR4-targeting properties and pharmacokinetic profile of the pentixafor backbone. A facile and fast one-pot $^{18}$F-labeling method, which uses complexation of $Al^{18}F^{2+}$ by macrocyclic chelators, such as NOTA or 1,4,7-triazacyclononane-1,4-diacetate (NODA) (33-35), and thus circumvents complex multistep syntheses, has been initially described by McBride et al. (36). However, because this $^{18}$F-labeling chemistry requires a cyloazanonane chelator instead of the larger 1,4,7,10-tetraazacyclododecane-1,4,7,10-tetraacetic acid (DOTA), and because the pentixafor scaffold is highly sensitive with respect to structural modifications, a slightly modified peptide analog, pentixather (Figure 1), was used to successfully merge the respective radiolabeling and CXCR4-targeting concepts. The pentixather scaffold has been shown to provide enhanced flexibility with respect to ligand modification in previous studies (37, 38); therefore, it was used for NOTA and alternative NCS-Bz-NODA conjugation.

## METHODOLOGY

### Synthesis of [$^{nat}$F]AlF-NOTA-Pentixather

The CPCR4.2 scaffold was synthesized according to a previously published protocol (39). NOTA was preactivated using *N*-hydroxysuccinimide (NHS), 1-ethyl-3-(3-dimethylaminopropyl) carbodiimide (EDC), and *N*-*N*-diisopropylamine (DIPEA) in water and coupled to the peptide (40). After successful coupling and purification, iodination was performed using a previously described procedure (41).

### Labeling of NOTA-Pentixather With $^{nat}$F$^-$

The labeling was performed using $AlCl_3$ and NaF (2 mM each) solutions in 0.5 M sodium acetate buffer (pH = 4). $AlCl_3$ (2.51 mmol; 1.20 equivalents), NaF (2.51 mmol; 1.20 equivalents), and ethanol (ETOH; 70% volume/volume [v/v]) were added to 2 mM of NOTA-pentixather (2.09 mmol in 0.5 M NaAc; pH = 4; 1.0 equivalents) and heated to 105°C for 20 minutes. The peptide was purified via reversed phase high-performance liquid chromatography (C18; 5 $\mu$m; 125 × 4.0 mm$^2$); 25%–45% MeCN in $H_2O$; 0.1% trifluoroacetic acid [v/v]; 15 minutes; $t_R$ = 13.5 minutes) to afford pure [$^{nat}$F]AlF-NOTA-pentixather. NOTA-pentixather HPLC (30% in 15 minutes: $t_R$ = 6.8 minutes. Electrospray ionization mass spectrometry [ESI-MS]: calculated for (C56H72IN13O12): 1245.5; found: m/z = 1246.7 $[M + H]^+$, 1268.6 $[M + Na]^+$. [$^{nat}$F]AlF-NOTA-pentixather HPLC (27% in 15 minutes): $t_R$ = 12.4 minutes. ESI-MS: calculated for (C56H70AlFIN13O12): 1289.4; found: m/z = 1291.0 $[M + H]^+$.

### Synthesis and Al[natF] Labeling of NODA-NCS-Pentixather

2,2′-(7-(4-isothiocyanatobenzyl)-1,4,7-triazonane-1,4-diyl) diacetic acid (NCS-Bn-NODA; 1.9 mg, 5.4 μmol, and 1.5 equivalents) was coupled to the CPCR4.2 scaffold (3 mg, 3.6 μmol, and 1 equivalent) using DIPEA (1.1 μL, 3.2 μmol, and 2 equivalents) in anhydrous *N*,*N*-dimethylformamide to obtain pH ≈ 9. Upon completion, the product was iodinated and purified. [natF]AlF-labeling was performed as described above, using DMSO (70% [v/v]). NODA-NCS-pentixather HPLC (20%–50% in 15 minutes): $t_R$ = 10.6 minutes; ESI-MS: calculated for (C54H70IN13O10S): 1219.4; found: m/z = 1220.7 $[M + H]^+$, 1242.4 $[M + Na]^+$. [natF]AlF-NODA-NCS-pentixather HPLC (20%–50% in 15 minutes): $t_R$ = 9.8 minutes. ESI-MS: calculated for (C54H68AlFIN13O10S): 1263.4; found: m/z = 1264.6 $[M + H]^+$, 1286.4 $[M + Na]^+$.

### [natGa]3+ Labeling of NOTA-Pentixather

A solution of $Ga(NO_3)_3$ (250 μL, 2 mM, and 1 equivalent) in water (pH = 3) was added to the peptide (250 μL, 2 mM, and 1 equivalent). For chelation of $Ga^{3+}$, mixtures were heated at 90°C for 30 minutes. HPLC and ESI-MS revealed quantitative complexation. [natGa]NOTA-pentixather HPLC (30%–55% in 15 minutes): $t_R$ = 12.3 minutes. ESI-MS: calculated for (C56H70GaIN13O12): 1312.4; found: m/z = 1312.7 $[M + H]^+$.

### Radiolabeling

For radiolabeling, $^{18}F^-$ was eluted from a Chromabond PS-$HCO_3$ cartridge in $K_2CO_3$ (34.5 mM, pH = 11) or sodium acetate (0.5 M, pH = 4) and added to a solution containing 10 μL of aqueous $AlCl_3$ (1 mM in 0.5 M NaOAc, pH = 4, 10 nmol), 10 μL of aqueous NOTA-pentixather (2 mM in $H_2O$:DMSO), 1:1 [v/v], 20 nmol), and DMSO (70% [v/v]). The pH was adjusted to 4 by the addition of acetic acid, and the reaction mixture was heated to 105°C for 15 minutes. The radiolabeled peptide was purified using a SepPak C8 light cartridge (Waters, Milford, Connecticut) to remove unreacted $^{18}F^-$ and DMSO. In brief, the labeled peptide was applied on the cartridge and washed with 10 mL of $H_2O$. The radiolabeled peptide was then eluted with EtOH, affording radiochemical purities of >98% for [18F]AlF-NOTA-pentixather. Before injection in mice, EtOH was fully evaporated and the peptide was redissolved in phosphate-buffered saline (PBS) and 5% (v/v) EtOH. For $^{68}$Ga-labeling, [68Ga]pentixafor was prepared on a fully automated system (Scintomics GmbH) similar to that previously described (42). The$^{68}$Ge/$^{68}$Ga generator eluate was added to 5 nmol of peptide, buffered in HEPES buffer (pH = 7.4), and reacted for 5 minutes at 95°C (pH ~3–4). A Sep-Pak C8 light cartridge was used for purification.

### Lipophilicity

The octanol–water partition coefficient ($logP_{octanol/water}$) of [18F]AlF-NOTA-pentixather was determined as previously reported (43).

### Serum Stability

[18F]AlF-NOTA-pentixather was incubated in human serum (90 minutes; 37°C), and the samples were centrifuged to separate the plasma from the blood cells. Plasma proteins were removed by precipitation with acetonitrile (10 minutes; 4°C) and subsequent centrifugation and ultrafiltration. The blood sample was then determined by HPLC analysis.

### Cell Culture

For in vitro experiments, hCXCR4-transfected Chem-1 and Jurkat T-cell lines were used. The Jurkat cells were maintained in RPMI 1640 medium (Biochrom, Berlin) containing 10% fetal calf serum (Biochrom, Berlin). Chem-1 cells were cultured in Dulbecco's Modified Eagle Medium (Biochrom, Berlin) supplemented with 10% fetal calf serum, 1% non-essential amino acids (Biochrom, Berlin), and 1% HEPES (1 M). Both cell lines were cultured at 37°C in humidified atmosphere with 5% $CO_2$ and passaged 2 to 3 times a week, depending on the cell count and confluency.

### Determination of $IC_{50}$

CXCR4 affinities were determined through competitive binding assays using Jurkat T-cells with [125I]FC131 as the radioligand. The Jurkat cells ($4 \times 10^5$ cells per vial) were incubated with the respective peptide of interest at final concentrations ranging from $10^{-11}$ M to $10^{-5}$ M and approximately 0.1 nM [125I]FC131. The total sample volume was 250 μL. After an incubation time of 120 minutes, the vials were centrifuged at 300 rcf (1300 rmp; Heraeus Megafuge, Thermo) for 3 minutes and the supernatant was removed. Cells were washed twice with 200 μL ice-cold hanks' balanced salt solution (HBSS; Biochrom, Berlin). After each washing step, the samples were centrifuged and the supernatant was removed. The amount of free radioligand in the combined supernatants and bound radioligand in the cell pellet was quantified. $IC_{50}$ values were determined using GraphPad Prism software (GraphPad Software, Inc., California).

### Internalization Studies

Chem-1 cells (150 000 cells/well) were seeded in 24-well plates 1 day before the experiment. On the day of the experiment, the culture medium was removed, cells were washed and incubated with 200 μL of the assay medium (Dulbecco's Modified Eagle Medium-F12, 5% BSA) at 37°C for a minimum of 15 minutes. Further, either 25 μL of the assay medium (total binding, n = 3) or 25 μL of 100 μM AMD3100 (nonspecific binding, n = 3) was added to the wells, followed by 25 μL of 10 nM [18F]AlF-NOTA-pentixather or [68Ga]pentixafor. After an incubation time of up to 60 minutes, the 24-well plates were placed on ice for 1 minute to halt internalization. Subsequently, the supernatant was removed, and the cells were washed with 250 μL of ice-cold PBS. The combined supernatant and PBS fractions represent the amount of free radioligand. To remove membrane-/receptor-bound radioligand, cells were washed twice with 250 μL of ice-cold acid wash (0.02 M NaOAc in saline, buffered with AcOH to pH = 5) and fractions were combined. Internalized activity was released by cell lysis using 250 μL of NaOH; further, the wells were washed with 250 μL of PBS. Fractions were combined again, and the quantification of free, membrane-bound, and internalized activity was performed using a γ-counter.

### Cell Efflux Studies

[18F]AlF-NOTA-pentixather was added to Chem-1 cells, and internalization was allowed for 1 hour at 37°C. Subsequently, the supernatant was removed, and the cells were washed and

incubated with 250 μL of the assay medium. At specific time points, the procedure, as described in the internalization assay, was repeated to determine retained intracellular activity.

### Biodistribution

All animal studies were approved by local authorities and are in compliance with the institution's guidelines. In this study, 5-week-old female CB17 severe combined immunodeficient (SCID) mice (Charles River Laboratories) were subcutaneously injected in the right shoulder with 0.1 mL matrigel containing $1 \times 10^7$ cells/mL Daudi human B-cell lymphoma cells. Five weeks after the inoculation, when the tumor size reached ~5–10 mm in diameter, 300 kBq of $^{18}$F-labeled peptide (195 pmol, 0.251 μg, and specific activity [SA] ≥1.54 GBq/μmol) was intravenously administered (n = 4) into the tail vein of isoflurane-anesthetized animals. The CXCR4 specificity was shown in a separate competition study through coinjection of 2 mg/kg AMD3100. After PET/computed tomography imaging, the mice were sacrificed (68 minutes post injection [p.i.]). Subsequently, the tissues and organs of interest were dissected, weighed, and counted for radioactivity in a γ-counter. The percentage of injected dose per gram of tissue (% ID/g) was calculated.

### PET/Computed Tomography

Mice were anesthetized using isoflurane anesthesia and injected with 300 kBq (195 pmol, 0.251 μg, and ≥4.86 GBq/μmol) of [$^{18}$F]AlF-NOTA-pentixather via the tail vein in 100 μL of PBS/5% (v/v) EtOH. For the blocking study, an additional group of mice (n = 4) was coinjected with 2 mg/kg AMD3100. PET scans were performed using an Inveon Siemens PET Scanner. The mice were placed on a platform inside the μPET scanner 1 hour p.i., and static images were acquired for 20 minutes. The images were reconstructed by a 2-dimensional ordered subset expectation maximum (2D-OSEM) algorithm with no correction applied for attenuation. Image analysis was performed using the Inveon software, and the results were calculated as % ID/g.

## RESULTS

### Al$^{18}$F Labeling

Scheme 1 shows the labeling procedure of NOTA-pentixather. In initial experiments, [$^{18}$F]fluoride (80-450 MBq) was eluted in a carbonate buffer (pH = 11), added to the reaction mixture, and adjusted to pH = 4.0. Under these conditions, [$^{18}$F]AlF-NOTA-pentixather was obtained in specific activities (SAs) of 2.45 ± 0.95 GBq/μmol at the end of the synthesis. Elution of [$^{18}$F]fluoride with the acetate buffer (pH = 4.0) leads to improved SAs of 7.15, 15.4, and 24.8 GBq/μmol for starting activities of 320, 1320, and 1500 MBq $^{18}F^-$, respectively. Radiochemical yields of 45.6% ± 13.3% were achieved, and the radiochemical purity of [$^{18}$F]AlF-NOTA-pentixather was 98.0% ± 1.7%.

### Synthesis of [$^{nat}$F]AlF-NOTA-Pentixather

[$^{nat}$F]AlF-labeling of NOTA and NODA-NCS-pentixather in an aqueous solution was not quantitative and afforded both the respective $Al^{3+}$-labeled and the desired $AlF^{2+}$-labeled species. Only when Al$^{nat}$F labeling was carried out in the solvent systems containing either 70% DMSO or 70% ETOH (v/v), [$^{nat}$F]AlF-NOTA- and [$^{nat}$F]AlF-NODA-NCS-pentixather were obtained in yields of 59% and 90%, respectively. The peptides were purified via preparative HPLC and used for in vitro binding studies (purity >95%).

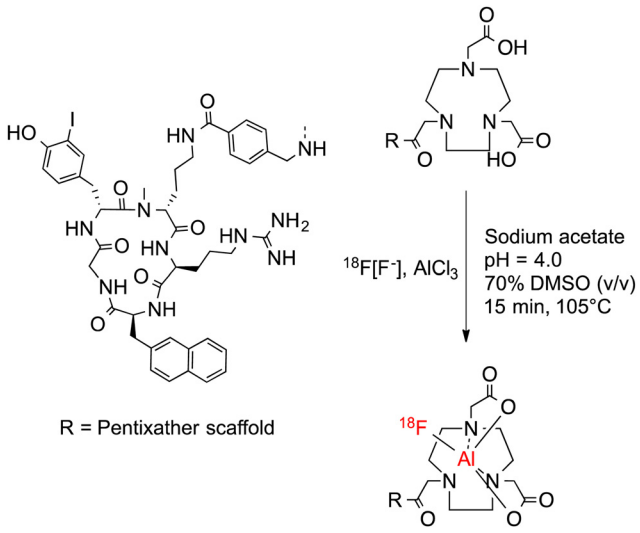


**Scheme 1.** Aqueous radiofluorination of NOTA-pentixather.

### Determination of Octanol–Water Partition Coefficient ($logP_{octanol/water}$)

[$^{18}$F]AlF-NOTA-pentixather shows a logP value of −1.4. Therefore, it is less hydrophilic than the DOTA-analog [$^{68}$Ga]pentixafor (logP = −2.9), which bears an additional carboxylate group compared with NOTA.

### Serum Stability

[$^{18}$F]AlF-NOTA-pentixather was incubated in human serum for 90 minutes at 37°C and analyzed by radio-HPLC. No instability was detected after 90 minutes.

### Determination of CXCR4 Affinities ($IC_{50}$)

CXCR4-affinities of the novel [$^{nat}$F]AlF-labeled analogs (Figure 1) and their uncomplexed precursors are summarized in Table 1 and

**Table 1** CXCR4 Affinities ($IC_{50}$) of the Novel [$^{nat}$F]AlF-NOTA and [$^{nat}$F]AlF-NODA-NCS-Pentixather Analogs, the Reference [$^{nat}$Ga]Pentixafor, and the Corresponding Uncomplexed Peptides

| Compound | $IC_{50}$ [nM] |
|---|---|
| Pentixafor | 102 ± 16 |
| [$^{nat}$Ga]pentixafor | 24.8 ± 2.5 |
| NOTA-pentixather | 27.5 ± 2.1 |
| [$^{nat}$F]AlF-NOTA-pentixather | 17.9 ± 0.2 |
| NODA-NCS-pentixather | 100 ± 15 |
| [$^{nat}$F]AlF-NODA-NCS-pentixather | 302 ± 77 |

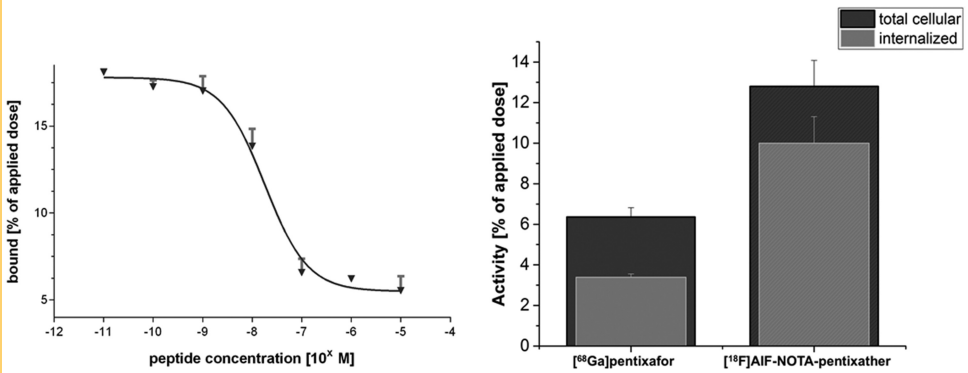


**Figure 2.** Representative competitive binding curve of [natF]AlF-NOTA-pentixather using Jurkat T-cells and [125I]FC131 as the radioligands (left panel), as well as total cellular uptake and internalization of [18F]AlF-NOTA-pentixather, compared with [68Ga]pentixafor in hCXCR4-transfected Chem-1 cells (right panel). Data are corrected for nonspecific binding/internalization in the presence of 100 μM AMD3100.

compared with the reference [natGa]pentixafor. [natF]AlF-NOTA-pentixather shows a 1.4-fold increased affinity toward CXCR4, whereas the affinity of the NODA-NCS analog is significantly decreased. As observed for pentixafor, the affinity of free NOTA-pentixather is decreased compared with that of the corresponding [natF]AlF-NOTA peptide. Interestingly, however, this effect is reversed in the case of the NODA-NCS conjugate.

## Internalization and Efflux Studies

Figure 2 shows the CXCR4-specific total cellular uptake and internalization of [18F]AlF-NOTA-pentixather and the reference [68Ga]pentixafor into Chem-1 cells stably transfected with hCXCR4. Based on its enhanced CXCR4 affinity, [18F]AlF-NOTA-pentixather showed a 2-fold increase in the total cellular uptake after 60 minutes compared with [68Ga]pentixafor. Furthermore, the amount of internalized activity was enhanced by a factor of 3 for [18F]AlF-NOTA-pentixather. This is occasioned by an enhanced internalization efficiency of the [18F]AlF-labeled analog; almost 80% of the total cellular [18F]AlF-NOTA-pentixather activity was found to be internalized, as opposed to 53% for [68Ga]pentixafor. Cell efflux studies of [18F]AlF-NOTA-pentixather revealed intracellular retention of 45.5% ± 4.02% and 40.5% ± 3.46% after 30 and 60 minutes, respectively.

## Biodistribution and Small-Animal PET Imaging

Comparative biodistribution data for [18F]AlF-NOTA-pentixather (1 hour p.i.; n = 4) and [68Ga]pentixafor (1.5 hours p.i.; n = 6) in Daudi lymphoma-bearing SCID mice are summarized in Figure 3. Compared with [68Ga]pentixafor, [18F]AlF-NOTA-pentixather showed delayed blood clearance (1.98% ± 0.31% ID/g vs 0.97% ± 0.34% ID/g for [68Ga]pentixafor) and consequently higher uptake in non-target organs at 60 minutes p.i. Because of the increased lipophilicity of [18F]AlF-NOTA-pentixather, a shift towards hepatobiliary excretion and thus an increased nonspecific accumulation in the liver, gall bladder and intestines was observed. Furthermore, higher bone activity levels (2.7% ± 0.13% ID/g) were observed for [18F]AlF-NOTA-pentixather, which may be indicative of partial in vivo defluo-

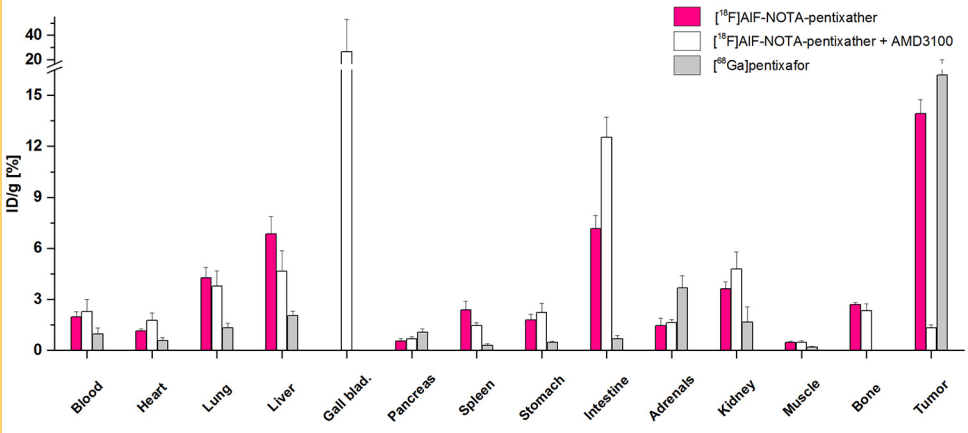


**Figure 3.** Biodistribution of [18F]AlF-NOTA-pentixather (60 minutes post injection [p.i.], n = 4, red bars) and [68Ga]pentixafor (1.5 hour p.i., n = 6, gray bars) in Daudi xenograft-bearing CB-17 SCID mice. To show CXCR4-specific tumor accumulation of [18F]AlF-NOTA-pentixather, 50 μg of AMD3100 was coinjected (60 minutes p.i., n = 4, white bars). Data are given in % ID/g tissue and are means ± SD.

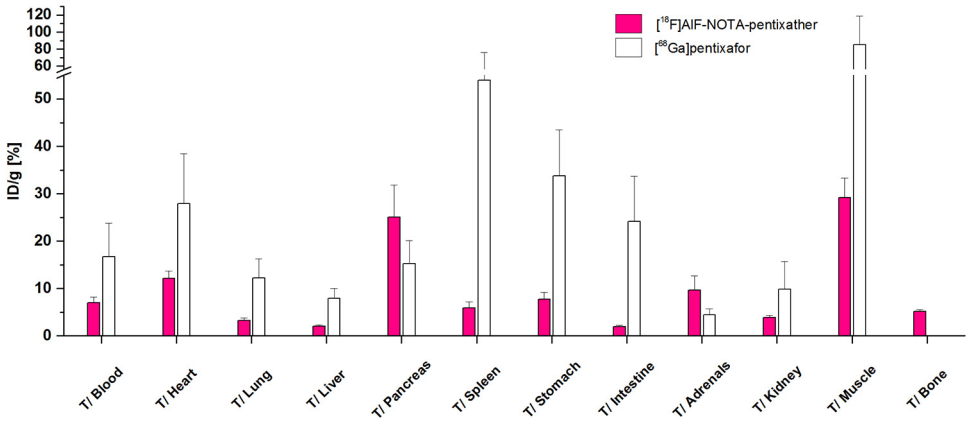


**Figure 4.** Tumor-to-organ ratios of [18F]AlF-NOTA-pentixather (red bars) compared with those of [68Ga]pentixafor (white bars). Data are expressed as mean ± SD (n = 4).

rination of the [18F]AlF-NOTA complex. Tumor accumulation of [18F]AlF-NOTA-pentixather was higher than the uptake in any other organ (14% ± 1% ID/g) and almost identical to that of [68Ga]pentixafor; respective tumor-to-organ ratios are shown in Figure 4. CXCR4 specificity of [18F]AlF-NOTA-pentixather uptake in the lymphoma xenograft was confirmed by coinjection of AMD3100, which reduced the tumor uptake by 91% (white bars, Figure 3). Coinjection of AMD3100 also reduced the uptake in the liver and spleen by 32% and 40%, respectively.

Representative PET images of [18F]AlF-NOTA-pentixather in Daudi lymphoma-bearing SCID are shown in Figure 5. As anticipated from the biodistribution data, [18F]AlF-NOTA-pentixather showed efficient CXCR4 receptor targeting (Figure 5A) and thus high uptake in the Daudi xenograft. As shown by the coinjection of 50 $\mu$g AMD3100 (Figure 5B), tumor accumulation

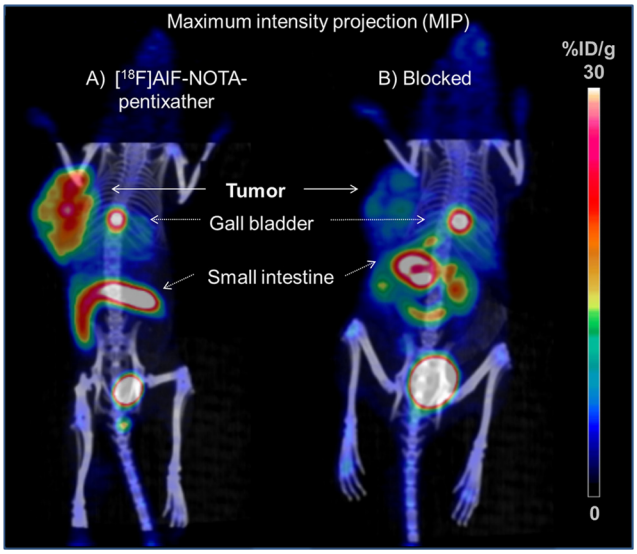


**Figure 5.** [18F]AlF-NOTA-pentixather PET/CT images of Daudi xenograft-bearing CB-17 SCID mice at 60 minutes p.i.; tracer only (A) and coinjection of 2 mg/kg AMD3100 (B). Mice were injected with 0.30 MBq of [18F]AlF-NOTA-pentixather (corresponding to 195 pmol/0.251 $\mu$g peptide).

of [18F]AlF-NOTA-pentixather was almost exclusively mediated by CXCR4. Besides the high tracer uptake in the tumor, strong [18F]AlF-NOTA-pentixather accumulation was only observed for the gall bladder and the intestines. Low, but discernible, activity uptake in the bones was also found.

## DISCUSSION

Since the discovery of CXCL12, the identification of CXCR4 as a coreceptor for HIV infection, and in particular the involvement of the CXCR4/CXCL12 axis in tumor progression and metastasis, the interest in the development of CXCR4-targeted tracers for diverse molecular imaging applications has significantly increased. Among these, the DOTA-functionalized cyclopeptide [68Ga]pentixafor represents a key development, as it allows high-contrast PET imaging of CXCR4 expression in vivo; thus, it is currently entering clinical trials (20-23, 44, 45).

However, based on its highly optimized structure, labeling pentixafor with other nuclides, for example, $In^{3+}$, results in a significant loss in CXCR4 affinity (18). In a recent study, we could show that small structural modifications in the peptide backbone, leading to pentixather (38, 41), provide a molecular scaffold with much higher flexibility toward structural modification and consequently a greater bandwidth of possible radiolabeling strategies.

To show this concept's sustainability, we aimed at combining the excellent CXCR4-targeting characteristics of pentixather-based tracers with a facile and rapid one-pot radiofluorination method based on $AlF^{2+}$ chelation, initially described by McBride et al. (46). Thus, pentixather was conjugated with 2 alternative chelators suitable for complexation of the $AlF^{2+}$ cation, namely, NODA (33) and NOTA, whereas the latter was evaluated in vitro and in vivo.

Although radiofluorination via [18F]$AlF^{2+}$ complexation has been widely used for the $^{18}F$ labeling of biomolecules in recent years, for example, the kit radiofluorination of somatostatin or integrin-targeting peptides (47, 48), representing a well-established radiofluorination strategy, some minor adjustments of radiolabeling conditions were performed to obtain [18F]AlF-NOTA-pentixather in satisfactory yields and sufficient SAs for in vivo application.

As depicted in Scheme 1, radiofluorination of NOTA-pentixather was performed with cyclotron-produced [18F]fluoride. Initially, $^{18}F^-$ was eluted from an anion exchange column using

a carbonate buffer (pH = 11). Because accurate pH adjustment to pH = 4 is essential for high radiochemical yields and the reaction volumes need to be kept to a minimum (<0.5 mL), pH adjustment after the addition of [18F]fluoride is critical. Initially, radiochemical yields of 45.6% ± 13.3% were achieved albeit with high inter-experimental variance and low SAs (2.45% ± 0.96% GBq/μmol). Upon changing the elution buffer to sodium acetate (preadjusted to pH = 4), only a slight pH adjustment after the addition of DMSO was necessary, and 18F-labeling resulted in 1.7-fold improved SAs. Scaling up to high starting activities (>1 GBq) was successful and resulted in SAs of up to 24.8 GBq/μmol. Moreover, the addition of DMSO significantly increased labeling yields, which is in accordance with previous studies (34). In summary, the chelation of [18F]AlF by NOTA-pentixather in an aqueous solution and the subsequent cartridge purification of the radiopharmaceutical was robust and straightforward and was completed within <30 minutes without requiring time-consuming drying steps. Particularly in the present case, where the targeted biomolecule does not allow ample structural adjustments to the requirements of the labeling chemistry, [18F]AlF complexation has distinct advantages over alternative innovative radiofluorination strategies. For example, silicon–fluoride acceptor or $BF_3$-based radiofluorination (49) also allows the fast, 1-step production of 18F-labeled tracers in high yields and high specific activities. However, fluoroborates are unstable toward hydrolysis and specific backbones have to be introduced to stabilize the trifluoroborate unit (50-53). Silicon–fluoride acceptor-based tracers require lipophilic silanol/silane precursors for radiofluorination, and lipophilicity-reducing structural components are required for enhanced pharmacokinetics in vivo (54-58). Hence, both methods involve the introduction of bulky and/or lipophilic groups, and thus, their applicability for the 18F-labeling of pentixafor/pentixather-based CXCR4 ligands is precluded or at least would require careful tracer optimization to balance the effect of the newly introduced functional groups on CXCR4 affinity and pharmacokinetics.

In this study, the minor structural modifications that have substantial effects on the CXCR4 affinity are appropriately illustrated by the comparison of the 2 novel pentixather analogs NOTA- and NODA-NCS-pentixather (Table 1). The latter was included in this study because higher [18F]$AlF^{2+}$ labeling efficiencies have been reported for NODA than for NOTA (33). However, this modification led to a considerable loss in CXCR4 affinity, whereas NOTA conjugation was well tolerated. This may be occasioned by the unfavorable shortening of the linker unit between the peptide core and the chelator by a carboxamide group. This structural deviation may lead to a loss of electrostatic interactions between the charged chelate and the receptor-binding pocket, thus reducing the receptor affinity of the NODA-NCS analog. The spacer length between the peptide and the chelate is a critical parameter for high-affinity CXCR4 binding as observed in previous studies on pentixafor analogs with variable spacers (18).

However, the [natF]AlF-NOTA analog showed a 1.4-fold improved CXCR4 affinity compared with [natGa]pentixafor (Table 1). Thus, it is important to note that in contrast to previous studies, higher cell numbers were used for the $IC_{50}$ experiments in this study ($4 \times 10^5$ vs $2 \times 10^5$ cells/sample); therefore, absolute $IC_{50}$ values for [natGa]pentixafor differ between reports (18). Surprisingly, although [18F]AlF-NOTA-pentixather showed an improved CXCR4 affinity and a 3-fold increased internalization compared with [68Ga]pentixafor, in vivo tumor uptake of both compounds was found to be nearly identical. This is attributed to the substantially different overall pharmacokinetics of [18F]AlF-NOTA-pentixather vs [68Ga]pentixafor, resulting in the reduced availability of the radiofluorinated tracer for CXCR4 targeting.

Obviously, because of its higher logP value of −1.4 ([68Ga]pentixafor: logP = −2.9), [18F]AlF-NOTA-pentixather showed higher plasma protein binding than [68Ga]pentixafor and hence delayed blood clearance. As visible in the PET images (Figure 5), this results in enhanced accumulation in the hepatobiliary system and thus higher background activity levels in the abdominal region compared with [68Ga]pentixafor (19). Because of the uptake of [18F]AlF-NOTA-pentixather in the liver and gall bladder of 6.9% ± 1.0% ID/g, the use for clinical imaging of liver metastasis can therefore be limited. However, interestingly, hepatic clearance into the gall bladder was very fast, resulting in comparably low tracer uptake in the liver and high focal activity accumulation in the gall bladder and the intestines at 60 minutes p.i.

Besides some nonspecific tracer uptake in the excretion organs, relatively high activity levels in bone (2.7% ± 0.7% ID/g) were also observed. This was attributed to a small degree of in vivo defluorination of the [18F]AlF-NOTA complex. Interestingly, a similar bone uptake of 2.95% ± 0.74% ID/g was reported for [18F]AlF-NOTA-T140, a T140 analog with high affinity toward human and murine CXCR4 (29). In that case, however, bone uptake was shown to be partially mediated by targeting of endogenously expressed mCXCR4 in bone marrow, and coinjection of 100 μg of the unlabeled compound reduced bone uptake by ~50%. In the case of [18F]AlF-NOTA-pentixather (Figure 3), coinjection of AMD3100 did not significantly influence bone activity levels, and thus specific targeting to mCXCR4-expressing cells in the bone marrow does not seem to significantly contribute to the overall 18F activity in bone.

Interestingly, accumulation of [18F]AlF-NOTA-pentixather in other CXCR4-expressing tissues, for example, spleen, was partially blocked by the coinjection of 50 μg AMD3100 (Figure 3). This hints toward reduced hCXCR4 selectivity of [18F]AlF-NOTA-pentixather compared with that of [68Ga]pentixafor, and thus some binding affinity to mCXCR4. However, this hypothesis needs to be confirmed in additional binding studies using mCXCR4-expressing cells.

The evaluation of [18F]AlF-NOTA-pentixather showed that, for the first time, a pentixather derivative could be labeled with 18F for high-contrast PET imaging of CXCR4 expression in vivo. Suitable CXCR4-targeting properties of [18F]AlF-NOTA-pentixather were exemplified by high-contrast delineation of CXCR4-positive human xenografts in a mouse model, and the applicability of the pentixather scaffold for the implementation of novel labeling strategies was shown.

Furthermore, the fast and facile one-pot Al18F-fluorination of [18F]AlF-NOTA-pentixather makes the tracer ideally suited for kit formulation and hence clinical transfer. However, for this, further studies regarding the in vivo stability and slight pharmacokinetic optimization are necessary.

## ACKNOWLEDGMENTS

The authors wish to thank M. Herz, for the supply of $^{18}F$, S. Reder and M. Mittelhäuser for PET imaging, V. Felber for [$^{not}F$]-labeling, and S. Hintze, C. Kiwus, and M. Konrad for synthetic assistance. We thank J. Notni and I. Laitinen for supportive and fruitful discussions.

The research leading to these results received funding from the Deutsche Forschungsgemeinschaft (DFG), collaborative research center SFB 824, subproject Z1 and B5.

Disclosure: Hans-Jürgen Wester is a shareholder at Scintomics.

Conflict of Interest: None Reported.

## REFERENCES

1. Tamamura H, Tsutsumi H, Masuno H, Fujii N. Development of low molecular weight CXCR4 antagonists by exploratory structural tuning of cyclic tetra- and pentapeptide-scaffolds towards the treatment of HIV infection, cancer metastasis and rheumatoid arthritis. Curr Med Chem. 2007;14(1):93–102.
2. Kuil J, Buckle T, van Leeuwen FW. Imaging agents for the chemokine receptor 4 (CXCR4). Chem Soc Rev. 2012;41(15):5239–5261.
3. Domanska UM, Kruizinga RC, Nagengast WB, Timmer-Bosscha H, Huls G, de Vries EGE, Walenkamp AME. A review on CXCR4/CXCL12 axis in oncology: no place to hide. Eur J Cancer. 2013;49(1):219–230.
4. Bridger GJ, Skerlj RT, Thornton D, Padmanabhan S, Martellucci SA, Henson GW, Abrams MJ, Yamamoto N, De Vreese K, Pauwels R. Synthesis and structure-activity relationships of phenylenebis(methylene)-linked bis-tetraazamacrocycles that inhibit HIV replication. Effects of macrocyclic ring size and substituents on the aromatic linker. J Med Chem. 1995;38(2):366–378.
5. Tamamura H, Xu Y, Hattori T, Zhang X, Arakaki R, Kanbara K, Omagari A, Otaka A, Ibuka T, Yamamoto N, Nakashima H, Fujii N. A low-molecular-weight inhibitor against the chemokine receptor CXCR4: a strong anti-HIV peptide T140. Biochem Biophys Res Commun. 1998;253(3):877–882.
6. Fujii N, Oishi S, Hiramatsu K, Araki T, Ueda S, Tamamura H, Otaka A, Kusano S, Terakubo S, Nakashima H, Broach JA, Trent JO, Wang ZX, Peiper SC. Molecular-size reduction of a potent CXCR4-chemokine antagonist using orthogonal combination of conformation- and sequence-based libraries. Angew Chem Int Ed Engl. 2003;42(28):3251–3253.
7. Hanaoka H, Mukai T, Tamamura H, Mori T, Ishino S, Ogawa K, Iida Y, Doi R, Fujii N, Saji H. Development of a 111In-labeled peptide derivative targeting a chemokine receptor, CXCR4, for imaging tumors. Nucl Med Biol. 2006;33(4):489–494.
8. Jacobson O, Weiss ID, Kiesewetter DO, Farber JM, Chen XY. PET of tumor CXCR4 expression with 4-F-18-T140. J Nucl Med. 2010;51(11):1796–1804.
9. Jin T, Tiwari DK, Tanaka S, Inouye Y, Yoshizawa K, Watanabe TM. Antibody-protein A conjugated quantum dots for multiplexed imaging of surface receptors in living cells. Mol Biosyst. 2010;6(11):2325–2331.
10. Leblond F, Davis SC, Valdes PA, Pogue BW. Pre-clinical whole-body fluorescence imaging: Review of instruments, methods and applications. J Photochem Photobiol B. 2010;98(1):77–94.
11. Jacobson O, Weiss ID, Szajek LP, Niu G, Ma Y, Kiesewetter DO, Farber JM, Chen X. PET imaging of CXCR4 using copper-64 labeled peptide antagonist. Theranostics. 2011;1:251–262.
12. Jacobson O, Weiss ID, Szajek LP, Niu G, Ma Y, Kiesewetter DO, Peled A, Eden HS, Farber JM, Chen X. Improvement of CXCR4 tracer specificity for PET imaging. J Control Release. 2012;157(2):216–223.
13. Khan A, Silversides JD, Madden L, Greenman J, Archibald SJ. Fluorescent CXCR4 chemokine receptor antagonists: metal activated binding. Chem Commun (Camb). 2007(4):416–418.
14. Jacobson O, Weiss ID, Szajek L, Farber JM, Kiesewetter DO. 64Cu-AMD3100–a novel imaging agent for targeting chemokine receptor CXCR4. Bioorg Med Chem. 2009;17(4):1486–1493.
15. Nimmagadda S, Pullambhatla M, Stone K, Green G, Bhujwalla ZM, Pomper MG. Molecular imaging of CXCR4 receptor expression in human cancer xenografts with [64Cu]AMD3100 positron emission tomography. Cancer Res. 2010;70(10):3935–3944.
16. De Silva RA, Peyre K, Pullambhatla M, Fox JJ, Pomper MG, Nimmagadda S. Imaging CXCR4 expression in human cancer xenografts: evaluation of monocyclam 64Cu-AMD3465. J Nucl Med. 2011;52(6):986–993.
17. Weiss ID, Jacobson O, Kiesewetter DO, Jacobus JP, Szajek LP, Chen X, Farber JM. Positron emission tomography imaging of tumors expressing the human chemokine receptor CXCR4 in mice with the use of 64Cu-AMD3100. Mol Imaging Biol. 2012;14(1):106–114.
18. Demmer O, Gourni E, Schumacher U, Kessler H, Wester HJ. PET imaging of CXCR4 receptors in cancer by a new optimized ligand. ChemMedChem. 2011;6(10):1789–1791.
19. Gourni E, Demmer O, Schottelius M, D'Alessandria C, Schulz S, Dijkgraaf I, Schumacher U, Schwaiger M, Kessler H, Wester HJ. PET of CXCR4 expression by a (68)Ga-labeled highly specific targeted contrast agent. J Nucl Med. 2011;52(11):1803–1810.
20. Wester HJ, Keller U, Schottelius M, Beer A, Philipp-Abbrederis K, Hoffmann F, Simecek J, Gerngross C, Lassmann M, Herrmann K, Pellegata N, Rudelius M, Kessler H, Schwaiger M. Disclosing the CXCR4 expression in lymphoproliferative diseases by targeted molecular imaging. Theranostics. 2015;5(6):618–630.
21. Philipp-Abbrederis K, Herrmann K, Knop S, Schottelius M, Eiber M, Luckerath K, Pietschmann E, Habringer S, Gerngross C, Franke K, Rudelius M, Schirbel A, Lapa C, Schwamborn K, Steidle S, Hartmann E, Rosenwald A, Kropf S, Beer AJ, Peschel C, Einsele H, Buck AK, Schwaiger M, Gotze K, Wester HJ, Keller U. In vivo molecular imaging of chemokine receptor CXCR4 expression in patients with advanced multiple myeloma. EMBO Mol Med. 2015;7(4):477–487.
22. Herrmann K, Lapa C, Wester HJ, Schottelius M, Schiepers C, Eberlein U, Bluemel C, Keller U, Knop S, Kropf S, Schirbel A, Buck AK, Lassmann M. Biodistribution and radiation dosimetry for the chemokine receptor CXCR4-targeting probe 68Ga-pentixafor. J Nucl Med. 2015;56(3):410–416.
23. Vag T, Gerngross C, Herhaus P, Eiber M, Philipp-Abbrederis K, Graner FP, Ettl J, Keller U, Wester HJ, Schwaiger M. First experience on chemokine receptor CXCR4 targeted positron emission tomography (PET) imaging in patients with solid cancers. J Nucl Med. 2016; pii: jnumed.115.161034. [Epub ahead of print].
24. Lapa C, Lückerath K, Kleinlein I, Monoranu CM, Linsenmann T, Kessler AF, Rudelius M, Kropf S, Buck AK, Ernestus RI, Wester HJ, Löhr M. K. H. 68Ga-Pentixafor-PET/CT for imaging of chemokine receptor 4 expression in glioblastoma. Theranostics. 2016;6(3):428–434.
25. Lapa C, Luckerath K, Rudelius M, Schmid JS, Schoene A, Schirbel A, Samnick S, Pelzer T, Buck AK, Kropf S, Wester HJ, Herrmann K. [68Ga]Pentixafor-PET/CT for imaging of chemokine receptor 4 expression in small cell lung cancer - initial experience. Oncotarget. 2016;7(8):9288–9295.
26. Thackeray JT, Derlin T, Haghikia A, Napp LC, Wang Y, Ross TL, Schafer A, Tillmanns J, Wester HJ, Wollert KC, Bauersachs J, Bengel FM. Molecular imaging of the chemokine receptor CXCR4 after acute myocardial infarction. JACC Cardiovasc Imaging. 2015;8(12):1417–1426.
27. Lapa C, Reiter T, Werner RA, Ertl G, Wester HJ, Buck AK, Bauer WR, Herrmann K. [(68)Ga]Pentixafor-PET/CT for imaging of chemokine receptor 4 expression after myocardial infarction. JACC Cardiovasc Imaging. 2015;8(12):1466–1468.
28. Zhang XX, Sun Z, Guo J, Wang Z, Wu C, Niu G, Ma Y, Kiesewetter DO, Chen X. Comparison of (18)F-labeled CXCR4 antagonist peptides for PET imaging of CXCR4 expression. Mol Imaging Biol. 2013;15(6):758–767.
29. Yan X, Niu G, Wang Z, Yang X, Kiesewetter DO, Jacobson O, Shen B, Chen X. Al[F]NOTA-T140 peptide for noninvasive visualization of CXCR4 expression. Mol Imaging Biol. 2016;18(1):135–142.
30. Demmer O, Gourni E, Schumacher U, Kessler H, Wester HJ. PET imaging of CXCR4 receptors in cancer by a new optimized ligand. Chemmedchem. 2011;6.
31. Åberg O, Pisaneschi F, Smith G, Nguyen Q-D, Stevens E, Aboagye EO. 18F-labelling of a cyclic pentapeptide inhibitor of the chemokine receptor CXCR4. J Fluor Chem. 2012;135:200–206.
32. George GP, Pisaneschi F, Stevens E, Nguyen QD, Aberg O, Spivey AC, Aboagye EO. Scavenging strategy for specific activity improvement: application to a new CXCR4-specific cyclopentapeptide positron emission tomography tracer. J Labelled Comp Radiopharm. 2013;56(13):679–685.
33. Shetty D, Choi SY, Jeong JM, Lee JY, Hoigebazar L, Lee YS, Lee DS, Chung JK, Lee MC, Chung YK. Stable aluminium fluoride chelates with triazacyclononane derivatives proved by X-ray crystallography and 18F-labeling study. Chem Commun (Camb). 2011;47(34):9732–9734.
34. D'Souza CA, McBride WJ, Sharkey RM, Todaro LJ, Goldenberg DM. High-yielding aqueous 18F-labeling of peptides via Al18F chelation. Bioconjug Chem. 2011;22(9):1793–1803.

35. McBride WJ, D'Souza CA, Sharkey RM, Karacay H, Rossi EA, Chang CH, Goldenberg DM. Improved 18F labeling of peptides with a fluoride-aluminum-chelate complex. Bioconjug Chem. 2010;21(7):1331–1340.
36. McBride WJ, Sharkey RM, Karacay H, D'Souza CA, Rossi EA, Laverman P, Chang CH, Boerman OC, Goldenberg DM. A novel method of 18F radiolabeling for PET. J Nucl Med. 2009;50(6):991–998.
37. Schottelius M, Osl T, Poschenrieder A, Herrmann K, Lapa C, Hoffmann F, Schwaiger M, Lassmann M, Buck A, Wester H. [177]Lu-pentixather: preclinical and first patient results with a highly promising CXCR4-directed endoradiotherapeutic agent. J Nucl Med. 2015;56(3):339.
38. Herrmann K, Schottelius M, Lapa C, Osl T, Poschenrieder A, Haenscheid H, Lueckerath K, Schreder M, Bluemel C, Knott M, Keller U, Schirbel A, Samnick S, Lassmann M, Kropf S, Buck A, Einsele H, Wester HJ, Knop S. First-in-man experience of CXCR4-directed endoradiotherapy with 177Lu- and 90Y-labelled pentixather in advanced stage multiple myeloma with extensive intra- and extramedullary disease. J Nucl Med. 2015.
39. Demmer O, Dijkgraaf I, Schottelius M, Wester HJ, Kessler H. Introduction of functional groups into peptides via N-alkylation. Org Lett. 2008;10(10):2015–2018.
40. Schottelius M, Schwaiger M, Wester HJ. Rapid and high-yield solution-phase synthesis of DOTA-Tyr(3)-octreotide and DOTA-Tyr(3)-octreotate using unprotected DOTA. Tetrahedron Lett. 2003;44(11):2393–2396.
41. Schottelius M, Konrad M, Osl T, Poschenrieder A, Wester H-J. An optimized strategy for the mild and efficient solution phase iodination of tyrosine residues in bioactive peptides. Tetrahedron Lett. 2015;56(47):6602–6605.
42. Demmer O, Dijkgraaf I, Schumacher U, Marinelli L, Cosconati S, Gourni E, Wester HJ, Kessler H. Design, synthesis, and functionalization of dimeric peptides targeting chemokine receptor CXCR4. J Med Chem. 2011;54(21):7648–7662.
43. Schottelius M, Poethko T, Herz M, Reubi JC, Kessler H, Schwaiger M, Wester HJ. First (18)F-labeled tracer suitable for routine clinical imaging of sst receptor-expressing tumors using positron emission tomography. Clin Cancer Res. 2004;10(11):3593–3606.
44. Dijkgraaf I, Demmer O, Schumacher U, Feldhaus S, Anton M, Brandau W, Schwaiger M, Kessler H, Wester H. J. CXCR4 receptor targeting for in-vivo imaging of metastases. J Nucl Med. 2008;49:103P-b.
45. Derlin T, Jonigk D, Bauersachs J, Bengel FM. Molecular imaging of chemokine receptor CXCR4 in non-small cell lung cancer using 68Ga-Pentixafor PET/CT: Comparison with 18F-FDG. Clin Nucl Med. 2016;41(4):e204–e205.
46. McBride WJ, Sharkey RM, Goldenberg DM. Radiofluorination using aluminum-fluoride (Al18F). EJNMMI Res. 2013;3(1):36.
47. Wan W, Guo N, Pan D, Yu C, Weng Y, Luo S, Ding H, Xu Y, Wang L, Lang L, Xie Q, Yang M, Chen X. First experience of 18F-alfatide in lung cancer patients using a new lyophilized kit for rapid radiofluorination. J Nucl Med. 2013;54(5):691–698.
48. McBride WJ, D'Souza CA, Karacay H, Sharkey RM, Goldenberg DM. New lyophilized kit for rapid radiofluorination of peptides. Bioconjug Chem. 2012;23(3):538–547.
49. Bernard-Gauthier V, Bailey JJ, Liu Z, Wangler B, Wangler C, Jurkschat K, Perrin DM, Schirrmacher R. From Unorthodox to Established: The Current Status of (18)F-Trifluoroborate- and (18)F-SiFA-Based Radiopharmaceuticals in PET Nuclear Imaging. Bioconjug Chem. 2016;27(2):267–279.
50. Liu Z, Hundal-Jabal N, Wong M, Yapp D, Lin KS, Benard F, Perrin DM. A new 18F-heteroaryltrifluoroborate radio-prosthetic with greatly enhanced stability that is labelled by 18F-19F-isotope exchange in good yield at high specific activity. Medchemcomm. 2014;5(2):171–179.
51. Liu Z, Pourghiasian M, Radtke MA, Lau J, Pan J, Dias GM, Yapp D, Lin KS, Benard F, Perrin DM. An organotrifluoroborate for broadly applicable one-step 18F-labeling. Angew Chem Int Ed Engl. 2014;53(44):11876–11880.
52. Liu Z, Radtke MA, Wong MQ, Lin KS, Yapp DT, Perrin DM. Dual mode fluorescent (18)F-PET tracers: efficient modular synthesis of rhodamine-[cRGD]2-[(18)F]-organotrifluoroborate, rapid, and high yielding one-step (18)F-labeling at high specific activity, and correlated in vivo PET imaging and ex vivo fluorescence. Bioconjug Chem. 2014;25(11):1951–1962.
53. Pourghiasian M, Liu Z, Pan J, Zhang Z, Colpo N, Lin KS, Perrin DM, Benard F. (18)F-AmBF3-MJ9: a novel radiofluorinated bombesin derivative for prostate cancer imaging. Bioorg Med Chem. 2015;23(7):1500–1506.
54. Lindner S, Michler C, Leidner S, Rensch C, Wangler C, Schirrmacher R, Bartenstein P, Wangler B. Synthesis and in vitro and in vivo evaluation of SiFA-tagged bombesin and RGD peptides as tumor imaging probes for positron emission tomography. Bioconjug Chem. 2014;25(4):738–749.
55. Litau S, Niedermoser S, Vogler N, Roscher M, Schirrmacher R, Fricker G, Wängler B, Wängler C. Next generation of SiFAlin-based TATE derivatives for PET imaging of SSTR-positive tumors: Influence of molecular design on in vitro SSTR binding and in vivo pharmacokinetics. Bioconjug Chem. 2015;26(12):2350–2359.
56. Niedermoser S, Chin J, Wangler C, Kostikov A, Bernard-Gauthier V, Vogler N, Soucy JP, McEwan AJ, Schirrmacher R, Wangler B. In vivo evaluation of F-18-SiFAlin-modified TATE: A potential challenge for Ga-68-DOTATATE, the clinical gold standard for somatostatin receptor imaging with PET. J Nucl Med. 2015;56(7):1100–1105.
57. Schirrmacher R, Bradtmoller G, Schirrmacher E, Thews O, Tillmanns J, Siessmeier T, Buchholz HG, Bartenstein P, Wangler B, Niemeyer CM, Jurkschat K. 18F-labeling of peptides by means of an organosilicon-based fluoride acceptor. Angew Chem Int Ed Engl. 2006;45(36):6047–6050.
58. Wangler C, Waser B, Alke A, Iovkova L, Buchholz HG, Niedermoser S, Jurkschat K, Fottner C, Bartenstein P, Schirrmacher R, Reubi JC, Wester HJ, Wangler B. One-step (1)(8)F-labeling of carbohydrate-conjugated octreotate-derivatives containing a silicon-fluoride-acceptor (SiFA): in vitro and in vivo evaluation as tumor imaging agents for positron emission tomography (PET). Bioconjug Chem. 2010;21(12):2289–2296.